Deciding the PHATE of Persister Cells: Trajectory Mapping of Drug Tolerance in Osteosarcoma

Tyler Center's Fellowship 2026 Final Deliverable

Meika Tomita | University of Tsukuba | University of California, San Diego

Introduction

Drug tolerant persister cells are a residual subpopulation of cancer cells that survive an otherwise effective therapeutic exposure through a reversible, non-mutational adaptation rather than through classical genetic resistance (Wang et al., 2025). Because DTPs are not defined by a fixed mutation, they are difficult to anticipate from genomic profiling alone, and are increasingly recognized as a common precursor state before relapse across various cancer types (Shen et al., 2020). By focusing on the cell's transcriptional mechanism into DTP, an avenue of therapeutics opens to intercept this sneaky state before resistance is fixed.

Osteosarcoma, the most common primary malignant bone tumor, has a subset of patients that present with metastatic osteosarcoma at diagnosis (Marko et al., 2016). These patients often have poor prognosis for further metastasis or even recurrence after treatment (Spraker-Perlman et al., 2019).

In some aggressive and drug resistant osteosarcomas, there have been findings of increased inosine monophosphate dehydrogenase (IMPDH) activity (Fellenberg et al., 2010). IMPDH catalyzes the rate-limiting conversion of inosine monophosphate (IMP) to xanthosine monophosphate (XMP); guanine monophosphate (GMP) is subsequently generated from XMP and eventually converted to GDP and then GTP (Hedstrom, 2009). Mycophenolic acid (MPA) is an IMPDH inhibitor that impedes this process, resulting in a reduction of the available nucleotide pool, and thereby impacting vital processes such as nucleic acid synthesis, cell proliferation, and signaling (Hedstrom, 2009). Thus, MPA has been shown to be a promising

therapeutic that has the potential to promote cancerous apoptosis and stop cell migration (Klangjorhor et al., 2020).

Currently, the prodrug of MPA, Mycophenolate mofetil (MMF), has been tested in a phase II multi-center clinical trial for osteosarcoma (ESMMO). These clinical trials however, did not demonstrate sufficient efficacy (Koonrungsesomboon et al., 2025). Therefore, the cell states that become drug tolerant and persist must be investigated for MPA to be fully implemented into care (Koonrungsesomboon et al., 2025).

Previously established DTP mechanisms have converged on the integrated stress response as a shared downstream mechanism like apoptotic pathways (Kalkavan et al., 2022) and kinase inhibitors (Sharma et al., 2010). However, what remains unknown is the characterization of purely metabolic/ nucleotide stress triggers and its transition into DTP. If nucleotide stress produces a different mechanism or follows the same, then a tailored therapeutic must be formulated accordingly to prevent recurrence.

To address this, a time-resolved bulk RNA-seq dataset across a 21 day MPA treatment course and a six day recovery phase was analyzed using PHATE trajectory embedding (Moon et al., 2019). Alongside this, differential expression analysis was utilized to map the transcriptional path that U2OS osteosarcoma cells follow in and out of MPA induced DTP. Candidate genes associated with this transition were cross referenced with an integrated stress response gene panel and validated by time course RT-qPCR against DMSO baseline controls. To evaluate whether the known MPA-IMPDH2 binding configuration remains stable, molecular dynamics simulation was used to assess the stability of this interaction.

Characterizing whether the integrated stress response is engaged by this metabolic trigger, and whether the resulting persister population fully reverts upon drug withdrawal, offers a starting point for evaluating whether nucleotide stress induced persistence represents a therapeutically distinct route into DTP formation or converges on mechanisms that are already established.

Methodology

Cell Culture and Treatment

The human osteosarcoma U-2 OS cell line (purchased from ATCC #HTB-96) was cultured in Dulbecco's Modified Eagle's Medium (DMEM, Gibco, 11965-092) supplemented with 10% Fetal Bovine Serum (FBS, Gibco, A5256701) and 1% Zell Shield (Minerva Biolabs, 13-0050) contamination preventive reagent (Miyamoto et al., 2021). Cells were maintained in a humidified environment at 37C with 5% CO2. Cells were seeded in 10-cm dishes at a density of 0.25×10^5 cells/mL. Twenty four hours after seeding, medium was replaced with DMEM containing 0.2% DMSO (drug vehicle) or the following: 10 µM Mycophenolic Acid (Selleck S2487), 15µM Dasatinib (Selleck, S1021), 4 µM PP242 (Torkinib, Selleck, S2218), 0.5 µM Torin1 (Merck, 475991-10MGCN), or 1µM AZD8055 (Selleck, S1555). Each treatment had a final DMSO concentration of 0.2% as well as the DMSO control. Medium was replaced every three days. Dasatinib is a well established src tyrosine kinase inhibitor drug (Fauziya et al., 2023) while the other three (PP242, Torin 1, and AZD8055) are all known mTOR inhibitors (Chresta et al., 2010; Thoreen et al., 2009; Hoang et al., 2012).

Cells were imaged daily using a Nikon Eclipse Ti2 confocal microscope, and confluency was quantified with advanced research NIS-Elements analysis software. Imaging was performed for both the RNAseq experiment, across all five treatments and DMSO controls (**Fig. 1A-E**), and during the separate validation experiment (**Fig. 1F**).

Bulk RNA sequencing was performed across four independent experiments (n = 4, as described in detail below). A separate, independent validation experiment was done using the same MPA dose, treatment timepoints, and culturing parameters (n = 3). In the validation experiment, RT-qPCR was performed. On Days 3, 21, and 27, cells were harvested for RNA extraction and cDNA synthesis. For the dishes maintained after 21 days, treatment was withdrawn and cultured in DMSO containing DMEM through Day 27.

The U2OS cells were an ideal model for DTP in terms of imaging and cell maintenance. Not only do they have highly reproducible growth rates, they possess adhesive characteristics and flat morphology for ease of high resolution, label-free, phase-contrast imaging of intracellular structures.

RNA Sequencing, Differential Expression Analysis, and Pathway Analysis

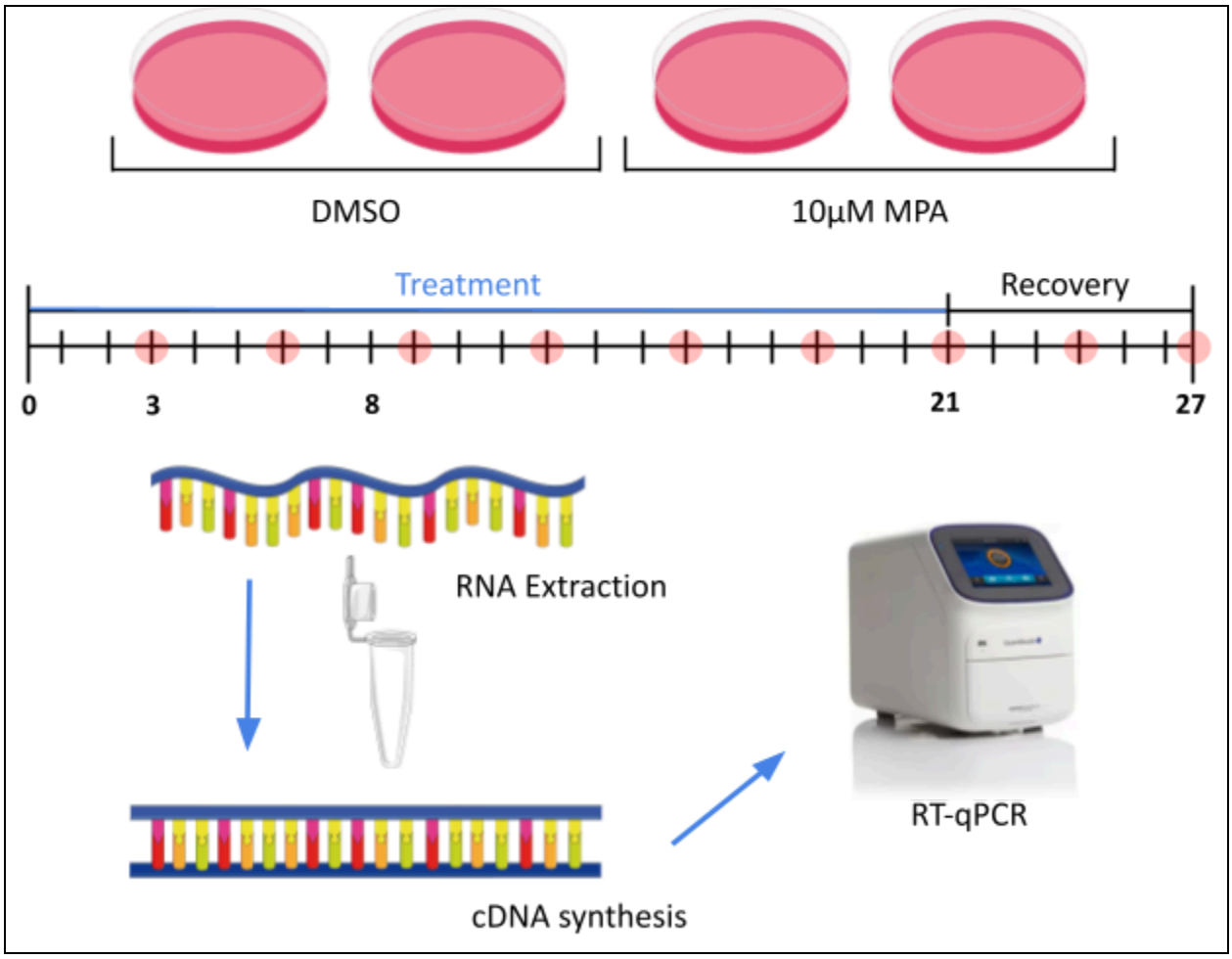
Bulk RNA sequencing was performed across four different independent experiments. In each experiment, the DMSO control was treated on Day 0 and collected on Day 3 (n = 4 total). For each of the five treatments (MPA, Dasatinib, PP242, Torin1, and AZD8055), samples were collected on Days 3, 8, 21, and 27 (n = 4 at each time point). For day 27 samples, the drug was withdrawn on Day 21 and a six day recovery period occurred before the final collection. Overall, there were 80 drug treated samples with 4 DMSO control samples, for a total of 84 samples.

Differential expression between consecutive timepoints (DMSO vs D3, D3 vs D8, D8 vs D21, D21 vs D27) and between the DMSO control and Day 21 and Day 27 was computed for the MPA treated samples using edgeR (Robinson et al., 2010). The thresholds followed standard guidelines for DEG analysis at FDR < 0.05 and |log2fold-change| > 1. Although DEGs tell the difference between the two experimental conditions, they do not directly mean they are the genes responsible for the DTP characteristics to appear. Thus, we utilized this information as a baseline for further investigation outlined in the future directions section.

Gene Ontology was used to identify potential pathways that could be activated based on the gene profile. Pathway activity and Hallmark gene set activity were inferred from the same pairwise comparisons using decoupler (Badia-i-Mompel et al., 2022).

Trajectory Analysis

Using Potential of Heat-diffusion for Affinity-based Trajectory Embedding analysis (PHATE) (Moon et al., 2019), gene profiles between treated vs untreated cells were mapped across the time points. The filtered expression matrix consisted of the top 40 variable genes with a nearest neighbor parameter of 5 (knn = 5) to build the initial local affinity graph. Rather than clustering via UMAP/PCA that conserves either local or global relationships, PHATE is able to preserve both simultaneously. Treatment timecourses must account for both as it is a continuous branching process. PHATE builds a diffusion-based affinity graph and then finds a low dimensional embedding that preserves local and geodesic distances; so the coordinates on a PHATE map are relevant to each other.



RT-qPCR Validation

RNA was extracted from 10µM MPA treated and DMSO control cells using the RNeasy Plus Mini Kit (Qiagen) with QIAshredder homogenization. RNA concentration and purity (A260/280, A260/230) were assessed by spectrophotometry (NanoDrop). cDNA was synthesized by normalizing RNA input using SuperScript III reverse transcriptase (Invitrogen) with oligo-dT priming, followed by RNase H treatment. cDNA was diluted to 5ng/µL as the qPCR input. Quantitative PCR was performed using SYBR Green chemistry on a Roche LightCycler 96, including a pre-incubation step, 40 cycles of PCR, and a melt curve analysis step.

A target gene panel of DDIT3, PPP1R15A (GADD34), TRIB3, ASS1, and HMOX1 was selected for the RT-qPCR validation. From the housekeeping genes ACTB, B2M, and GAPDH, stability was assessed by the pairwise-variation geNORM method (Vandesompele et al., 2002). GAPDH (M = 0.389) and B2M (M = 0.404) were selected as the most stable reference pair, while ACTB (M = 0.647) was excluded. The target gene expression was normalized to the geometric mean of GAPDH and B2M using the ddCt method, and fold-change was calculated relative to the DMSO control. Significance for RT-qPCR validated genes was assessed by two-tailed t-test on delta Ct values ($p<0.05$). Unlike the RNAseq DEG defining criteria above, there was no minimum fold-change threshold applied because the analysis was targeted and a pre-selected candidate panel rather than a genome-wide screen.

Molecular Dynamics Simulation

To evaluate if the MPA-IMPDH2 binding configuration remains stable in silico, MPA was docked into IMPDH2 (PDB: 1JR1) using AutoDock Vina (Trott & Olson, 2010), and the complex produced was simulated in three runs for 500 ns each using Desmond (Yoshino et al., 2019). Ligand stability, protein stability, and protein-ligand contact frequency were assessed across all three simulation runs.

Results

Figure 1. MPA induces a phenotype consistent with the drug-tolerant persister state.

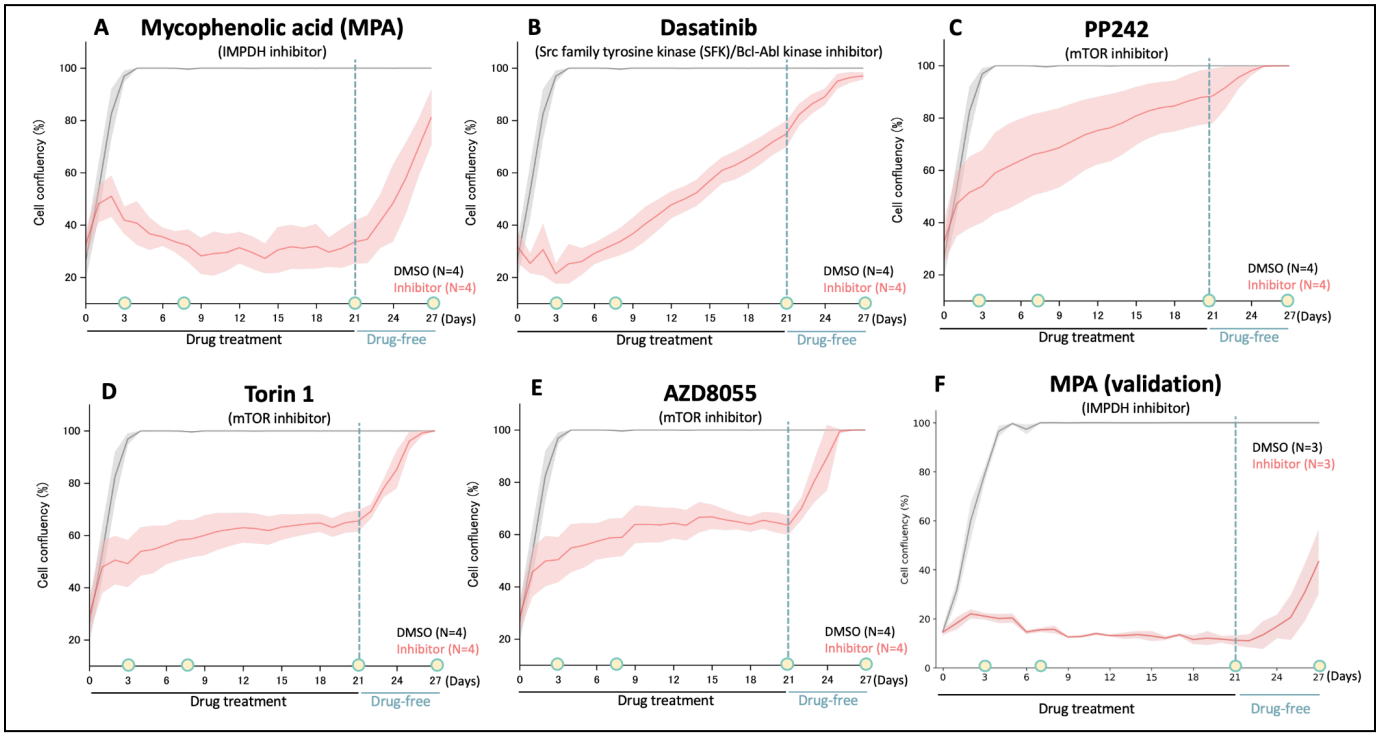


Fig 1 A*: Over a 21 day period, U-2 OS cells were treated with 10 µM Mycophenolic acid (MPA) with an initial response to MPA, decreased cell confluency. After 21 days, treatment is lifted and cells continue proliferation.* ***B****: Dasatinib treatment under the same 21 day course resulted in a continuous increase in cell confluency with or without treatment.* ***C****: mTOR inhibitor PP242 follows a gradual increase in cell confluency during the 21 day treatment course* ***D****: mTOR inhibitors Torin1 and* ***E****: AZD8055 slowly increase in cell confluency during the 21 day treatment but once the drugs are lifted, cell confluency increases exponentially.* ***F****: independent validation experiment (n = 3) confirming that the MPA induced a low confluency state during treatment and regrowth after drug withdrawal. This pattern mimicked cell confluency changes shown in panels A - E and therefore data were reproducible in a separately cultured cohort. The dashed*

line indicates Day 21 drug withdrawal. Cell confluency of MPA and DMSO were measured daily in U2OS cells.

Prior work has shown that MPA suppresses osteosarcoma proliferation and metastatic behavior (Klangjorhor et al., 2020), but whether this reflects a genuine persister phenotype (arrest through survival and regrowth vs simple growth inhibition) has not been fully characterized yet. To test this, U2OS cells were treated with MPA and four other drugs: Dasatinib and the mTOR inhibitors PP242, Torin1, AZD8055. DMSO control cells reached full confluency by Day 7 and remained there. MPA treated cells rose from 14.6% to 21.1% cell confluency by Day 3 and then declined and plateaued between 11.2% and 17.1% confluency for the remainder of the 21 day treatment course (**Fig 1F**.). This stable, quiescence-like arrest was then followed by a sharp increase in confluency after drug withdrawal from 16.9% at Day 24 to 43.3% at Day 27 (**Fig 1F**.). The Dasatinib treated cells proliferated regardless of treatment status; the mTOR inhibitors increased gradually under treatment with a comparatively slower increase after drug exposure. MPA treated cells exhibited the most behavioral signature DTP characteristics with the arrest then regrowth pattern. Thus, for the subsequent analyses, the MPA treated cells were focused on.

Figure 2. PHATE trajectory analysis suggests an apparent return to baseline.

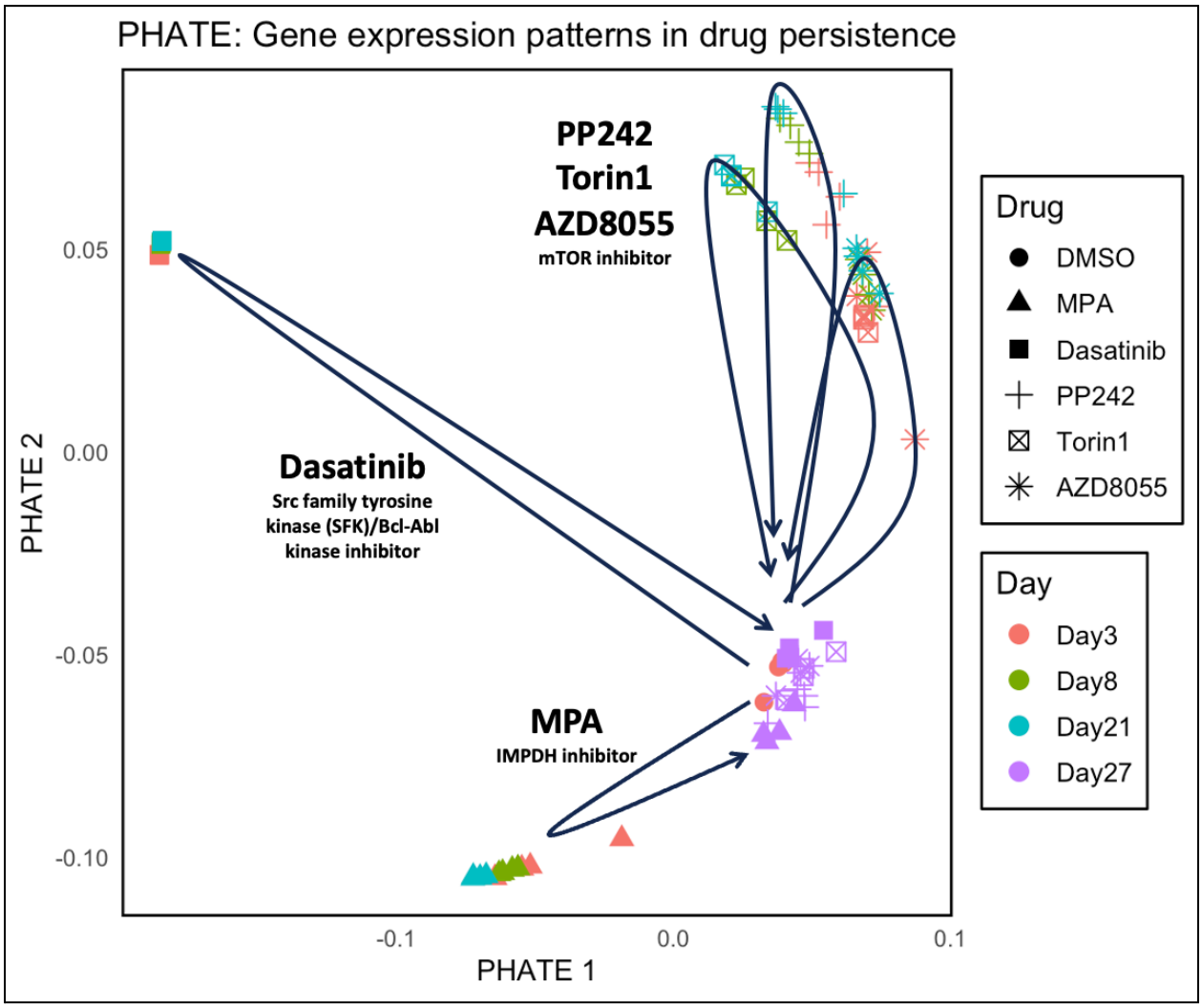


Fig 2*: Gene Expression Patterns in Drug Persistence. DMSO control, MPA, Dasatinib, PP242, Torin1, AZD8055 are depicted by their respective symbols. Each distinct day Day 3 - Day 27 are represented by their respective colors.*

PHATE trajectory embedding of the time resolved transcriptome showed Day 3 samples were positioned away from the untreated baseline region (DMSO control) toward a treatment associated region of the trajectory space. By Day 27 however, samples were positioned closer to

the baseline region. Simply by observation alone would suggest a general reversal of the transcriptional response. However, the subsequent sections complicate this observation.

Figure 3. Differential expression and Gene ontology analysis reveal coordinated cell-cycle arrest and re-entry.

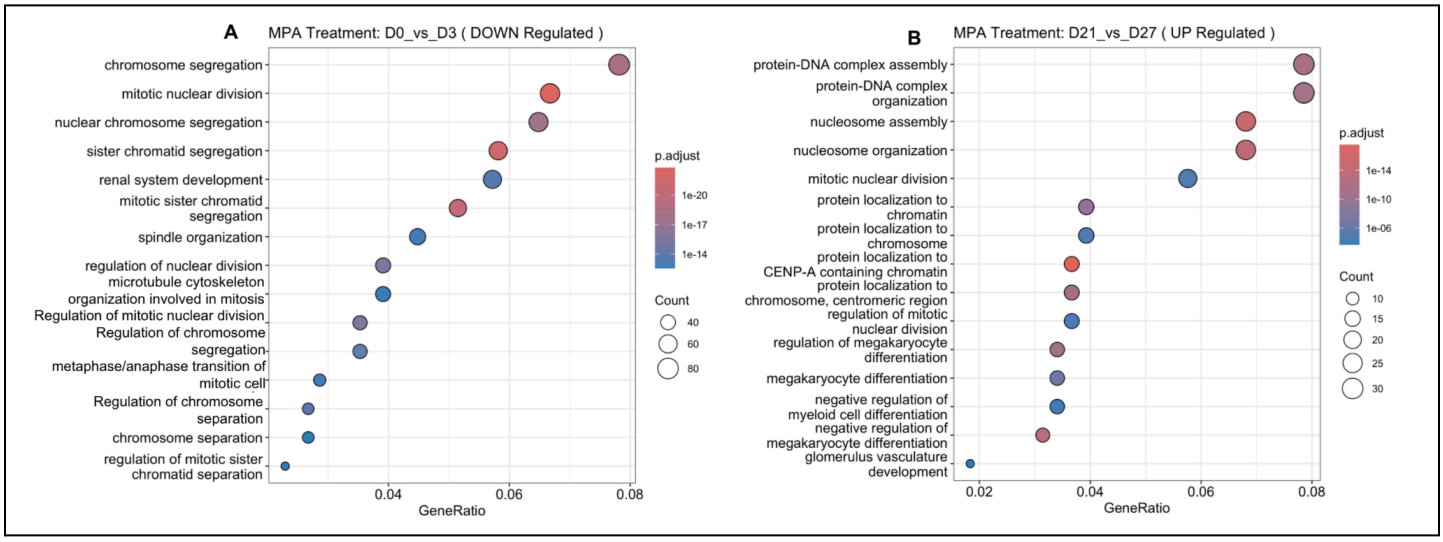


Fig 3. *Differential expression and Gene Ontology analysis reveal coordinated cell-cycle arrest and re-entry.* ***A****: Dot plots show biological process GO terms significantly enriched among downregulated genes at DMSO control vs Day 3* ***B****: and at Day 21 vs Day 27. Dot size depicts gene count per GO term and color indicates the corresponding adjusted p-value. Gene ratio is the proportion of the entire input gene list to the one term.*

Pairwise DEG analysis (edgeR; FDR<0.05, |log2FC|>1) across four consecutive time point transitions showed the transcriptome's largest shifts at the DMSO control to Day 3 transition (2,808 DEGs) and the Day 21 to Day 27 transition (1,240 DEGs). Comparatively, there were modest changes between the transition days Day 3 to Day 8 (138 DEGs) and Day 8 to Day 21 (80 DEGs). Gene Ontology analysis of the large shift transitions gave each their distinct biological

signature (**Fig. 3**) Genes downregulated in DMSO control vs D3 were a majority cell cycle and chromosome segregation GO terms directly consistent with the confluency arrest shown in **Fig. 1**. Genes upregulated at D21 vs D27 consisted of nucleosome assembly, protein-DNA complex assembly, and CENP-A containing chromatin localization terms, which were consistent with cells re-entering the cell cycle after drug withdrawal. This GO analysis was treated as an orienting, exploratory pass rather than primary evidence as GO terms only signify there is potential for biological significance and is unable to depict which pathways are actually being up/down regulated.

Figure 4 qPCR Gene Panel

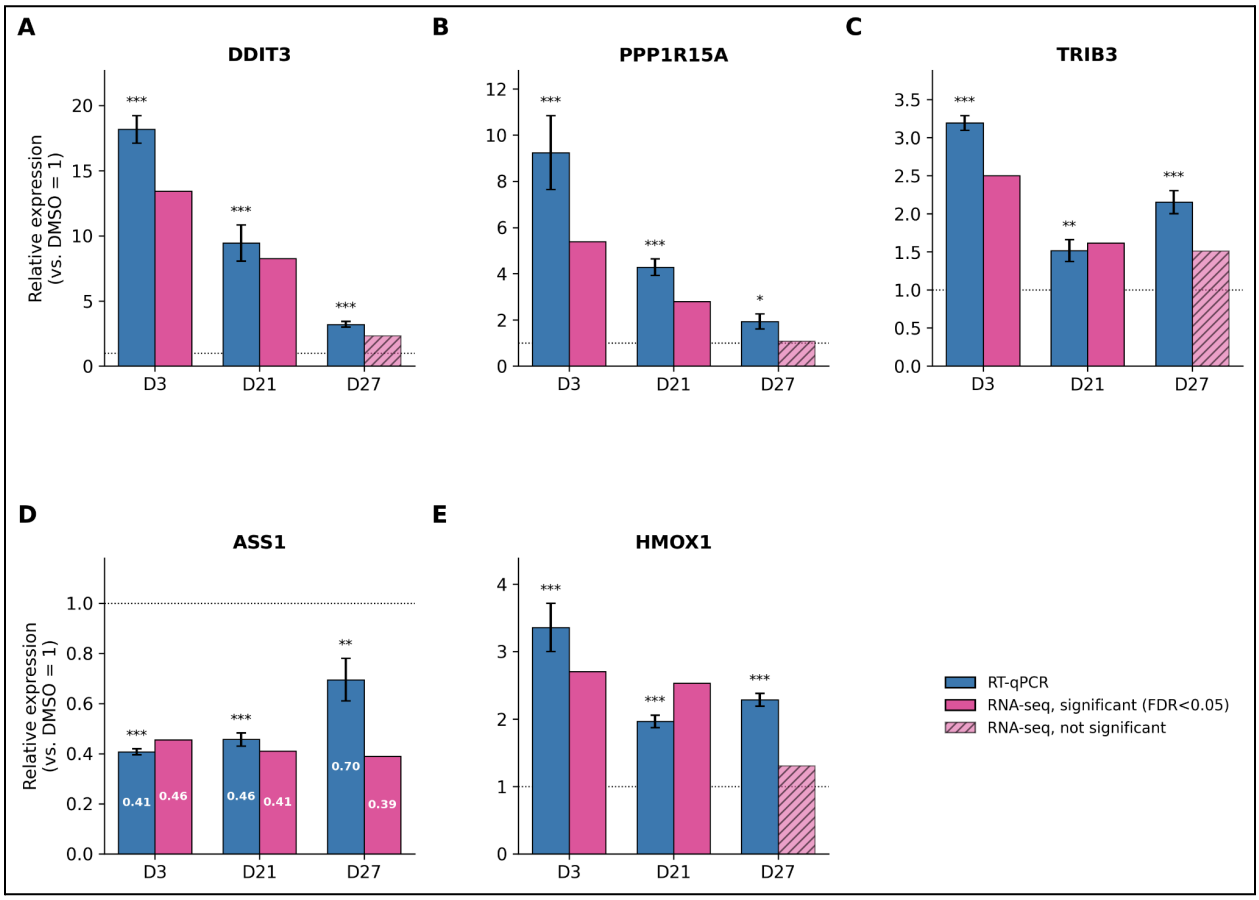


Fig 4. *The integrated stress response is acutely engaged and incompletely resolved, while ASS1 remains persistently repressed. RT-qPCR (blue) and RNA-seq (pink) relative expression of* ***A****: DDIT3,* ***B****: PPP1R15A,* ***C****: TRIB3,* ***D****: ASS1,* ***E****: HMOX1 in MPA treated U2OS cells, both expressed relative to DMSO control = 1. The controls were normalized to the geometric mean of B2M and GAPDH (the geNORM, most stable, validated reference pair). The qPCR bars show mean +/- STDEV (n = 3 biological replicates). Asterisk denote significance vs DMSO control by two-tailed t-test on delta Ct values (*p<0.05, **p<0.01, ***p<0.001). Solid pink bars indicate RNAseq FDR < 0.05; hatched pink bars indicate FDR ≥ 0.05.*

A five gene panel (DDIT3, PPP1R15A, TRIB3, ASS1, HMOX1) was validated by RT-qPCR, normalized to a geNORM selected reference pair of B2M and GAPDH (M = 0.389 and 0.404 vs ACTB with M = 0.65 and thus excluded for instability). DDIT3 (**Fig. 4A**), PPP1R15A (**Fig. 4B**), and TRIB3 (**Fig. 4C**) were all significantly upregulated at Day 3 relative to the DMSO controls (18.1 fold, 9.2 fold, and 3.2 fold respectively; all $p<0.001$). This is consistent with an acute ISR engagement under IMPDH induced nucleotide depletion. Rather than resolving fully at Day 27 (6 days after drug withdrawal), all three genes remained significantly elevated with DDIT3 at 3.2 fold ($p<0.001$), PPP1R15A a 1.9 fold ($p<0.05$), and TRIB3 a 2.2 fold ($p<0.001$). Although this reflects a decay in gene expression, it also shows an incomplete return to baseline. RNA-seq comparisons at the same timepoints showed the same direction of change for all three genes at Day 3 and Day 21 (FDR < 0.05), though this agreement did not reach statistical significance by Day 27 (**Fig. 4A-C**). On the other hand, ASS1 (**Fig. 4D**) showed an inverse pattern, remaining significantly downregulated at every timepoint (0.41 fold at Day 3, 0.46 fold at Day 21, 0.69 fold at Day 27; $p<0.01$ or better throughout). ASS1's repression was independently confirmed by

RNA-seq at all three time points (D3, D21, D27; all FDR < 0.05). HMOX1 (**Fig. 4E**) showed a similar pattern to the ISR related genes with a partially sustained expression level across all three time points (3.3 fold, 2.0 fold, 2.3 fold at Days 3, 21, 27 respectively; all p<0.001)

PROGENy pathway activity inference showed p53 pathway activation at D3 vs DMSO control (ULM score +32.2, p<0.001), Hallmark P53_PATHWAY scoring (+8.4, p<0.001), and Hallmark APOPTOSIS activation (+2.6, p<0.05). This is consistent with the p53 activation under nucleotide stress. The p53 pathway activity was negative at D27 to D21 (PROGENy -31.4; Hallmark -5.8, both p<0.001). Because this is only reflective of the D21 to D27 change rather than a direct comparison to the DMSO control, this decline is not evidence that p53 activity fully returns to its baseline. Consistent with this, several p53 target genes remained significantly elevated at DMSO control vs D27 through DEG analysis (**Table 1**). ASS1 (**Fig. 4D**), which has been reported as an intrinsic repressor of Akt in other cellular contexts (Miyamoto et al., 2017), was found to be consistently downregulated at DMSO control vs D21 (logFC = -1.28, FDR = 6.3×10^{-5}) and DMSO control vs D27 (logFC = -1.36, FDR=6.4×10^{-5}) with CPS1, a second urea-cycle enzyme (logFC = -0.98, FDR=9.9×10^{-5}). ASS1 expression is controlled by multiple mechanisms across cancer contexts, including HIF-1a mediated repression (Wen-Bin et al., 2009) and promoter methylation (Nicholson et al., 2009), in addition to p53. Akt activity was not directly assessed, so any downstream consequences for Akt signaling remain a hypothesis in this context.

Table 1. P53 target gene and urea-cycle enzyme expression DMSO control vs Day 27 (edgeR, FDR<0.05)

Gene	log2FC	FDR

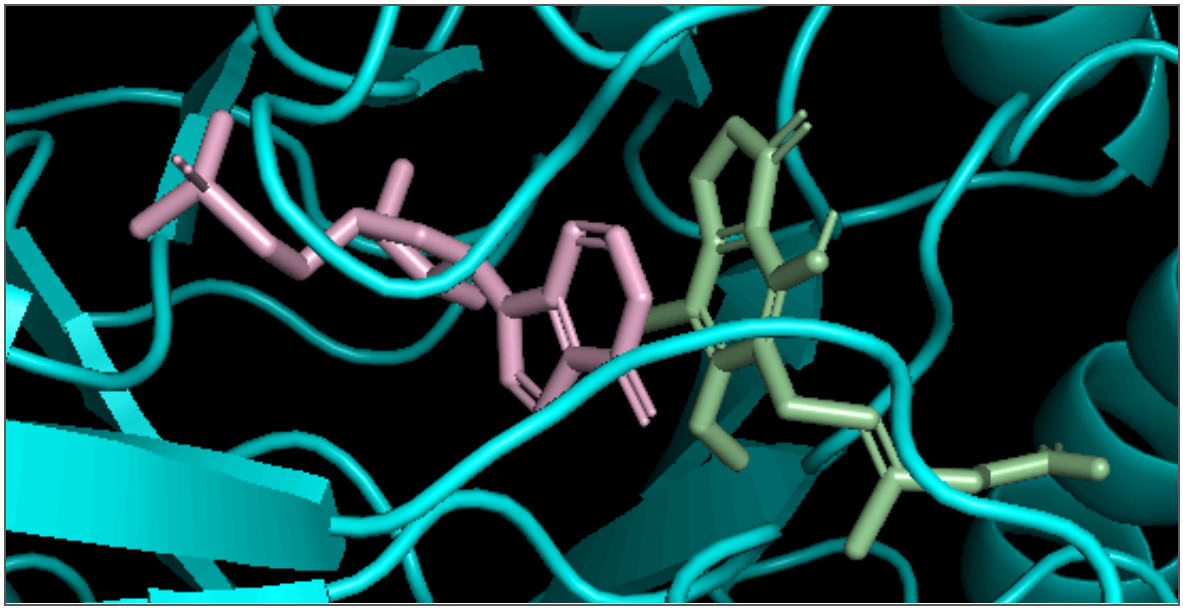
CDKN1A	+ 1.07	4.8×10^{-11}
MDM2	+ 1.02	5.6×10^{-13}
GADD45A	+ 1.14	9.5×10^{-6}
SESN1	+ 0.69	2.5×10^{-2}
SESN2	+ 0.89	5.5×10^{-4}
RRM2B	+ 0.68	3.9×10^{-7}
BTG2	+ 0.71	3.1×10^{-4}
ASS1	- 1.36	6.4×10^{-5}
CPS1	- 0.98	9.9×10^{-5}

Table 1 *outlines selected p53 target genes and urea-cycle genes with FDR < 0.05. Unlike the DEG criteria defined in the Methods section (FDR < 0.05 and |log2FC| > 1), no minimum log2FC threshold was applied here as these genes were selected based on prior biological relevance (canonical p53 targets and urea-cycle enzymes) rather than a genome wide screening. Positive log2FC indicates higher expression at Day 27 relative to DMSO control.*

Residual transcriptional signature after MPA withdrawal.

Direct comparison of Day 27 to the DMSO controls identified 935 significant DEGs, of which around 300 were not differentially expressed at any earlier time point. PHATE trajectory embedding (**Fig. 2**) and DEG analyses capture different aspects of transcriptional recovery at Day 27.

Figure 5. Molecular dynamics simulation of the MPA-IMPDH2 complex.



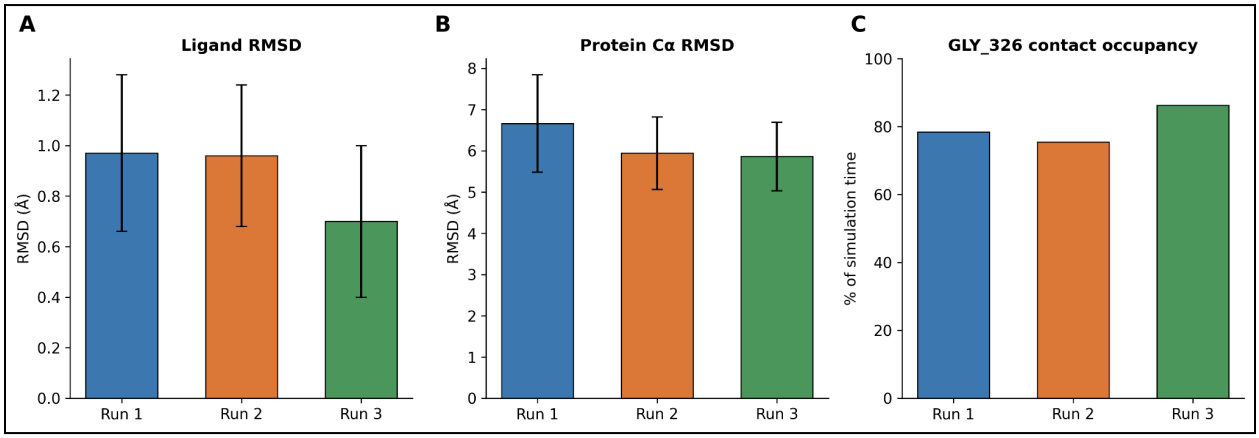


Fig. 5 *Mycophenolic Acid (Green) interacting with its target protein, Inosine Monophosphate Dehydrogenase 2 (snapshot from PyMol visualization). Three independent molecular dynamics simulations were run at 500 ns each.* ***A****: Ligand RMSD,* ***B*** *: protein Cα RMSD,* ***C****: GLY_326 contact occupancy were measured for each run.*

MPA + IMPDH MD Simulation

An in-silico examination of whether the known MPA-IMPDH2 binding configuration remains stable was performed through molecular dynamics simulations. Three runs were performed independently for 500ns each using Desmond. Across all three replicates, MPA

remained tightly bound within the IMPDH2 active site: the ligand RMSD was low and consistent across all three runs (**Fig. 5A**: 0.97 +/- 0.31 Å, 0.96 +/- 0.28 Å, 0.70 +/- 0.3 Å). These values are smaller than the protein's backbone flexibility (**Fig. 5B**: 6.66 +/- 1.18 Å, 5.94 +/- 0.88 Å, and 5.86 +/- 0.83Å), meaning that the MPA ligand does not drift or unbind out of its binding pocket even though it has some conformational movement somewhere else in the protein. The hydrogen bond in the backbone of GLY_326 was used as the most reproducible contact across all three runs (**Fig. 5C**: 78.4%, 75.4%, 86.2% of run time). This baseline supports the idea that the runs are consistent and reproducible.

Discussion & Future Directions

From this study, MPA induced nucleotide stress engages in similar ISR mechanisms previously defined by apoptotic pathway triggered persistence (Kalkavan et al., 2022) and kinase inhibitor induced persistence (Sharma et al., 2010). DDIT3, PPP1R15A, and TRIB3 were acutely increased at Day 3. Rather than resolving later on, they remained measurably elevated even six days after drug withdrawal. ISR engagement is supported during MPA induced persistence, however, it cannot be said that ISR is mechanistically required for MPA DTP formation. ASS1 has been previously reported to function as an intrinsic Akt repressor in other cellular contexts (Miyamoto et al., 2017). Its persistent loss raises the question of other upstream mechanisms that play a role in cell persistence under therapeutics. HMOX1 closely mimicked the ISR genes from the RT-qPCR panel indicating its acute induction likely reflects a general stress response rather than a distinct, sustained oxidative stress response.

The captured differences between the PHATE trajectory position and Day 27 vs DMSO control DEG analysis are a notable observation. However, both methods are sensitive to different features of the transcriptome (global manifold position vs gene level statistical difference). Although it appears that one measure resets, another substantial, partially novel signature appears. This corroborates the growing understanding that DTP cells may retain a molecular memory of prior drug exposure that is not completely erased after drug recovery (Wang et al., 2025).

Several limitations impacted interpretation of data. Bulk RNA sequencing cannot resolve if persistent signatures show a uniform response throughout the surviving population or a stronger signal within the persister subpopulation diluted by non-persister cells. GO analysis was used as an exploratory orientation of biological relevance of the DEGs identified rather than confirmed pathway activity. Molecular dynamics results support a stable MPA-IMPDH2 structure across independent runs but nevertheless remain a predictive structural model. All data were derived from a single cell line (U2OS) meaning the results cannot be directly generalized to other cancer types.

Establishing necessity for either ISR or ASS1 in DTP formation would require functional perturbation like a CRISPR knockout of ASS1, or a pharmacological ISR inhibition. This raises the natural next question: without ASS1, do cells lose the ability to enter the persister state, or does its loss have no functional effect on DTP formation? Defining a quantifiable metric of “DTP-ness” from the identified persister signature at Day 27 would allow this phenotype to be measured rather than only identified, and would support testing whether this mechanism generalizes to other cancer or treatments beyond osteosarcoma and MPA.

References

Badia-i-Mompel, P., Vélez Santiago, J., Braunger, J., Geiss, C., Dimitrov, D., Müller-Dott, S., Taus, P., Dugourd, A., Holland, C. H., Ramirez Flores, R. O., & Saez-Rodriguez, J. (2022). decoupleR: ensemble of computational methods to infer biological activities from omics data. Bioinformatics advances, 2(1), vbac016. https://doi.org/10.1093/bioadv/vbac016

Bulvas, O., Knejzlík, Z., Sýs, J. et al. Deciphering the allosteric regulation of mycobacterial inosine-5′-monophosphate dehydrogenase. Nat Commun 15, 6673 (2024). https://doi.org/10.1038/s41467-024-50933-6

Chresta, C. M. et al. AZD8055 is a potent, selective, and orally bioavailable ATP-competitive mammalian target of Rapamycin kinase inhibitor with in vitro and in vivo antitumor activity. Cancer Res. 70, 288–298. https://doi.org/10.1158/0008-5472.CAN-09-1751 (2010).

Fauziya, Gupta, A., Nadaf, A. et al. Dasatinib: a potential tyrosine kinase inhibitor to fight against multiple cancer malignancies. Med Oncol 40, 173 (2023). https://doi.org/10.1007/s12032-023-02018-5

Fellenberg, J., Kunz, P., Sähr, H., & Depeweg, D. (2010). Overexpression of inosine 5'-monophosphate dehydrogenase type II mediates chemoresistance to human osteosarcoma cells. PloS one, 5(8), e12179. https://doi.org/10.1371/journal.pone.0012179

Hedstrom L. (2009). IMP dehydrogenase: structure, mechanism, and inhibition. Chemical reviews, 109(7), 2903–2928. https://doi.org/10.1021/cr900021w

Hoang, B., Benavides, A., Shi, Y., Yang, Y., Frost, P., Gera, J., & Lichtenstein, A. (2012). The PP242 mammalian target of rapamycin (mTOR) inhibitor activates extracellular signal-regulated kinase (ERK) in multiple myeloma cells via a target of rapamycin complex 1 (TORC1)/eukaryotic translation initiation factor 4E (eIF-4E)/RAF pathway and activation is a mechanism of resistance. The Journal of biological chemistry, 287(26), 21796–21805. https://doi.org/10.1074/jbc.M111.304626

Kalkavan, H., Chen, M. J., Crawford, J. C., Quarato, G., Fitzgerald, P., Tait, S. W. G., Goding, C. R., & Green, D. R. (2022). Sublethal cytochrome c release generates drug-tolerant persister cells. Cell, 185(18), 3356–3374.e22. https://doi.org/10.1016/j.cell.2022.07.025

Klangjorhor, J., Chaiyawat, P., Teeyakasem, P., Sirikaew, N., Phanphaisarn, A., Settakorn, J., Lirdprapamongkol, K., Yama, S., Svasti, J., & Pruksakorn, D. (2020). Mycophenolic acid is a drug with the potential to be repurposed for suppressing tumor growth and metastasis in osteosarcoma treatment. International journal of cancer, 146(12), 3397–3409. https://doi.org/10.1002/ijc.32735

Koonrungsesomboon, N., Teeyakasem, P., Dukaew, N. et al. Efficacy and safety of mycophenolate mofetil in patients with high-grade locally advanced or metastatic

osteosarcoma (ESMMO): a multicenter, phase II clinical trial. Int J Clin Oncol 30, 2362–2374 (2025). https://doi.org/10.1007/s10147-025-02877-0

Marko, T. A., Diessner, B. J., & Spector, L. G. (2016). Prevalence of Metastasis at Diagnosis of Osteosarcoma: An International Comparison. Pediatric blood & cancer, 63(6), 1006–1011. https://doi.org/10.1002/pbc.25963

Miyamoto, T., Lo, P. H. Y., Saichi, N., Ueda, K., Hirata, M., Tanikawa, C., & Matsuda, K. (2017). Argininosuccinate synthase 1 is an intrinsic Akt repressor transactivated by p53. Science advances, 3(5), e1603204. https://doi.org/10.1126/sciadv.1603204

Miyamoto, T., Han, S. I., & Shimano, H. (2021). Protocol for rapid manipulation of mitochondrial morphology in living cells using inducible counter mitochondrial morphology (iCMM). STAR protocols, 2(3), 100721. https://doi.org/10.1016/j.xpro.2021.100721

Moon, K. R., van Dijk, D., Wang, Z., Gigante, S., Burkhardt, D. B., Chen, W. S., Yim, K., Elzen, A. V. D., Hirn, M. J., Coifman, R. R., Ivanova, N. B., Wolf, G., & Krishnaswamy, S. (2019). Visualizing structure and transitions in high-dimensional biological data. Nature biotechnology, 37(12), 1482–1492. https://doi.org/10.1038/s41587-019-0336-3

Nicholson, Linda J., et al. “Epigenetic Silencing of Argininosuccinate Synthetase Confers Resistance to Platinum-induced Cell Death but Collateral Sensitivity to Arginine Auxotrophy in Ovarian Cancer.” International Journal of Cancer. Journal International Du Cancer. [New York, NY], vol. 125, no. 6, Sept. 2009, pp. 1454–63, https://doi.org/10.1002/ijc.24546.

Robinson, M. D., McCarthy, D. J., & Smyth, G. K. (2010). edgeR: a Bioconductor package for differential expression analysis of digital gene expression data. Bioinformatics (Oxford, England), 26(1), 139–140. https://doi.org/10.1093/bioinformatics/btp616

Sharma, S. V., Lee, D. Y., Li, B., Quinlan, M. P., Takahashi, F., Maheswaran, S., McDermott, U., Azizian, N., Zou, L., Fischbach, M. A., Wong, K. K., Brandstetter, K., Wittner, B., Ramaswamy, S., Classon, M., & Settleman, J. (2010). A chromatin-mediated reversible drug-tolerant state in cancer cell subpopulations. Cell, 141(1), 69–80. https://doi.org/10.1016/j.cell.2010.02.027

Shen, S., Vagner, S., & Robert, C. (2020). Persistent Cancer Cells: The Deadly Survivors. Cell, 183(4), 860–874. https://doi.org/10.1016/j.cell.2020.10.027

Spraker-Perlman, H. L., Barkauskas, D. A., Krailo, M. D., Meyers, P. A., Schwartz, C. L., Doski, J., Gorlick, R., Janeway, K. A., & Isakoff, M. S. (2019). Factors influencing survival after recurrence in osteosarcoma: A report from the Children's Oncology Group. Pediatric blood & cancer, 66(1), e27444. https://doi.org/10.1002/pbc.27444

Thoreen, C. C., Kang, S. A., Chang, J. W., Liu, Q., Zhang, J., Gao, Y., Reichling, L. J., Sim, T., Sabatini, D. M., & Gray, N. S. (2009). An ATP-competitive mammalian target of rapamycin inhibitor reveals rapamycin-resistant functions of mTORC1. The Journal of biological chemistry, 284(12), 8023–8032. https://doi.org/10.1074/jbc.M900301200

Trott, O., & Olson, A. J. (2010). AutoDock Vina: improving the speed and accuracy of docking with a new scoring function, efficient optimization, and multithreading. Journal of computational chemistry, 31(2), 455–461. https://doi.org/10.1002/jcc.21334

Vandesompele, J., De Preter, K., Pattyn, F., Poppe, B., Van Roy, N., De Paepe, A., & Speleman, F. (2002). Accurate normalization of real-time quantitative RT-PCR data by geometric averaging of multiple internal control genes. Genome biology, 3(7), RESEARCH0034. https://doi.org/10.1186/gb-2002-3-7-research0034

Wang, Z., Wang, M., Dong, B. et al. Drug-tolerant persister cells in cancer: bridging the gaps between bench and bedside. Nat Commun 16, 10048 (2025). https://doi.org/10.1038/s41467-025-66376-6

Wen-Bin Tsai, Isamu Aiba, Soo-yong Lee, Lynn Feun, Niramol Savaraj, Macus Tien Kuo; Resistance to arginine deiminase treatment in melanoma cells is associated with induced argininosuccinate synthetase expression involving c-Myc/HIF-1α/Sp4. Mol Cancer Ther 1 December 2009; 8 (12): 3223–3233. https://doi.org/10.1158/1535-7163.MCT-09-0794

Yoshino, R., Yasuo, N., & Sekijima, M. (2019). Molecular Dynamics Simulation reveals the mechanism by which the Influenza Cap-dependent Endonuclease acquires resistance against Baloxavir marboxil. Scientific reports, 9(1), 17464. https://doi.org/10.1038/s41598-019-53945-1